Clinical Biomechanics 120 (2024) 106352

Contents lists available at ScienceDirect

Clinical Biomechanics

journal homepage: www.elsevier.com/locate/clinbiomech

Biomechanical modelling of indirect decompression in oblique lumbar intervertebral fusions – A finite element study

Mathieu Chayer [a,b], Philippe Phan [c], Pierre-Jean Arnoux [d], Zhi Wang [e,f], Carl-Éric Aubin [a,b,f,*]

[a] Institute of Biomedical Engineering, Polytechnique Montréal, PO Box 6079, Montreal, QC H3C 3A7, Canada
[b] Sainte-Justine University Hospital Center, Montreal, Canada
[c] Department of Surgery, Faculty of Medicine, University of Ottawa, Ottawa, ON, Canada
[d] Laboratoire de Biomécanique Appliquée, Aix-Marseille Université/Université Gustave Eiffel, Marseille, France
[e] Centre Hospitalier de l'Université de Montréal, Montreal, Canada
[f] Department of Surgery, Faculty of Medicine, Université de Montréal, Montreal, Canada

ARTICLE INFO

Keywords:
Lumbar spine surgery
Biomechanical study
Oblique lumbar interbody fusion (OLIF)
Finite element modelling
Indirect decompression

ABSTRACT

Background: Oblique lumbar intervertebral fusion aims to decompress spinal nerves via an interbody fusion cage, but the optimal surgical strategy, including implant selection for specific patient characteristics, remains unclear. A biomechanical model was developed to assess how pathophysiological characteristics and instrumentation impact spinal realignment, indirect decompression, and cage subsidence risk.

Methods: A finite element model of the L4-L5 segment was derived from a validated asymptomatic T1-S1 spine model. Five cases of grade I spondylolisthesis with normal or osteoporotic bone densities and initial disc heights of 4.3 to 8.3 mm were simulated. Oblique lumbar intervertebral fusion with cage heights of 10, 12, and 14 mm (12° lordosis) was examined. Postoperative changes in disc height, foraminal and spinal canal dimensions, segmental lordosis, and vertebral slip were assessed. Vertebral stresses and displacements under 10 Nm flexion and 400 N gravitational load were compared between stand-alone constructs and bilateral pedicle screw fixation using rods of 4.75, 5.5, and 6 mm diameters.

Findings: Oblique lumbar intervertebral fusion significantly improved postoperative disc height, foraminal and spinal canal dimensions, with the greatest enhancements observed with 14 mm cages. Bilateral pedicle screw fixation markedly reduced cortical endplate stresses and displacements compared to stand-alone constructs, with added benefits from larger rod diameters. Low bone density increased displacements by 63 %.

Interpretation: Thicker cages achieve better decompression but increase subsidence risk. Bilateral pedicle screw fixation with 6 mm rods minimizes endplate stresses and displacements, especially in osteoporotic cases. Future research will validate these findings and explore the model's potential for surgical planning.

1. Introduction

Nowadays, some 620 million people suffer from back pain, representing a considerable socioeconomic burden (Ferreira et al., 2023). Degenerative lumbar pathologies frequently cause significant back and leg pain, and in severe cases, surgical interventions such as intervertebral fusion are used to treat these conditions. Among the various fusion techniques, oblique lumbar interbody fusion (OLIF) has gained popularity for its potential to restore disc height, achieve spinal realignment, and provide indirect decompression of lumbar spinal nerves. OLIF is a minimally invasive surgical approach used to treat various degenerative lumbar pathologies, including degenerative disc disease, degenerative spondylolisthesis, and spinal stenosis. Unlike traditional posterior or anterior approaches, OLIF involves accessing the intervertebral disc space through a lateral retroperitoneal approach, obliquely entering the disc space between adjacent lumbar vertebrae, limiting the risk of intraoperative nerve injury (Hao et al., 2023). A key component of the OLIF procedure is the use of interbody cages, which are implanted into the intervertebral disc space with the purpose of restoring the disc height. Subsequently, the achieved correction can be secured using diverse fixation systems, including lateral plate systems and/or bilateral pedicle screw (BPS) fixation. A significant concern during OLIF procedures is the occurrence of cage subsidence, which may result in a loss of correction, decompression of neural elements and necessitate revision

* Corresponding author at: Institute of Biomedical Engineering, Polytechnique Montréal, PO Box 6079, Montreal, QC H3C 3A7, Canada.
E-mail address: carl-eric.aubin@polymtl.ca (C.-É. Aubin).

https://doi.org/10.1016/j.clinbiomech.2024.106352
Received 17 June 2024; Accepted 18 September 2024
Available online 20 September 2024

surgery. Additionally, despite its benefits, the optimal surgical strategy including best implants for a given patient characteristics is not yet well defined.

Recent experimental studies have emphasized the importance of evaluating the efficacy and identifying predictive indicators for indirect decompression in OLIF procedures. Sato et al. (2017) explored the clinical outcomes of OLIF in patients with lumbar spondylolisthesis, and found significant improvements in disc height, spinal canal diameter, and foraminal area post-surgery, accompanied by reductions in back and leg pain. Similarly, Xu et al. (2023) demonstrated the potential of OLIF through a comparison of geometric indicators, such as disc height, spinal canal volume, and cross-sectional area, among 16 patients who underwent OLIF with pedicle screw fixation. Using similar comparison parameters, another study found that inserting the cage in a more anterior position was correlated with an increased postoperative lordosis, while a more posterior positioning resulted in greater decompression (Mahatthanatrakul et al., 2022). Lastly, Iwasaki et al. (2022) reported a negative relationship between preoperative posterior disc height and the change in antero-posterior spinal canal diameter, ultimately suggesting that OLIF should be avoided in patients with preserved dorsal disc height.

While experimental studies offer a direct assessment of surgical outcomes for specific realistically analogous scenarios, they are often resource-intensive and limited in their ability to explore a wide range of parameters. In contrast, finite element (FE) analysis presents an alternative approach that complements experimental findings. FE studies offer the advantage of numerical experimentation in a controlled virtual environment, allowing for the exploration of numerous surgical scenarios, instrumentation options, and pathological conditions. Recent advancements in FE modelling have provided valuable insights into the biomechanics of OLIF. These studies have compared OLIF with other fusion approaches, including transforaminal lumbar interbody fusion (TLIF) and anterior lumbar interbody fusion (ALIF) (Lu and Lu, 2019; Ouyang et al., 2023), investigated the influence of instrumental options on stability (Zhang et al., 2023; Zhong et al., 2023), and assessed the risk of subsidence in relation to cage position (Qin et al., 2022) and bone density (Yang et al., 2022).

However, few models have incorporated pathological conditions or included indicators of decompression in their analysis, limiting the understanding of the quantitative compromise between realignment, decompression, and the risk of subsidence. This study seeks to develop a numerical biomechanical model to investigate the impact of different pathophysiological characteristics and instrumental options on spinal realignment, resulting decompression, and the risk of cage subsidence in OLIF procedures. Specifically, the focus of this study is to provide quantitative insights into the impact of different cage heights on achieved realignment (postoperative disc height, slip and lordosis), as well as spinal canal foraminal dimensions. Moreover, the study examines how cage heights, the utilization of BPS fixation, associated rod diameter, and bone density influence the stresses and displacements on cortical endplates, serving as indicators of the risk of cage subsidence.

2. Methods

2.1. Finite element modelling of the L4-L5 spinal functional unit

A detailed FEM of the L4-L5 segment previously developed and validated in the context of transforaminal lumbar interbody fusion (TLIF) was used as a base model in this study (Rastegar et al., 2020). This model is based on the Spine Model for Safety and Surgery (SM2S) which presents the geometry of a full spine reconstructed from CT-scan images of a 50th percentile asymptomatic man (El-Rich et al., 2009). The original model includes the vertebral bodies (cortical and trabecular bone), the intervertebral disc (nucleus pulposus (NP), annulus fibrosus (AF) and collagen fibres), and seven ligaments, i.e., the anterior longitudinal ligament (ALL), posterior longitudinal ligament (PLL), ligamentum flavum (LF), capsular ligaments (CL), intertransverse ligament (ITL), interspinous ligament (ISL) and supraspinous ligament (SSL) (Fig. 1A).

The vertebrae were meshed using 4-node tetrahedral elements to depict the inner trabecular bone surrounded by a cortical layer. This cortical layer exhibited variable thickness across five distinct regions: the endplates and anterior walls of the vertebral body (0.4 mm), upper pedicle (2 mm), lower pedicle (1.87 mm), posterior processes (1 mm), and the area where pedicle screws were inserted (0.8 mm), when applicable (Bianco et al., 2017). Regarding the intervertebral disc, the NP and AF were meshed using 8-node brick elements. The AF is represented by five concentric layers positioned between the adjacent vertebrae. These layers were augmented with spring elements acting in tension only to mimic the orientation of collagen fibres at ±35 degrees. Apart from the CL, which was meshed with 3-node shell elements, all ligaments were modeled using 4-node shell elements. The asymptomatic model of the L4-L5 functional unit contained a total of 988,411 nodes (464,278 elements).

Each structure was assigned corresponding material parameters, as shown in Table 1. The cortical and trabecular bone were modeled as homogeneous isotropic materials following the elastoplastic Johnson-Cook constitutive law. The NP and AF were represented using Mooney-Rivlin hyperelastic materials, while the response of the collagen fiber spring elements was implemented through tabulated force-displacement curves. The osteoporotic models were generated by decreasing the modulus of elasticity by 33 % for cortical bone and by 66 % for trabecular bone (Liu et al., 2022; Polikeit et al., 2003). General contacts with a 0.5 mm initial gap and Coulomb friction coefficient of 0.2 were used to model the facet joints and ligaments were attached to cortical bone through tied contacts (Bereczki et al., 2021; Guo et al., 2020). Prior research extensively validated mesh sizes, material properties, and contact definitions through mesh convergence studies and comparison of the range of motion (RoM) with experimental cadaveric studies (Rastegar et al., 2020; Wagnac et al., 2012).

2.2. Simulation of the OLIF procedure

From the base asymptomatic FEM, five pathologic models presenting a grade I spondylolisthesis with disc heights ranging from 4.3 to 8.3 mm were generated by translating L4 while maintaining L5 fixed in space. The OLIF procedure was simulated through a partial discectomy, involving the removal of elements from the discs to establish a corridor that traverses the intervertebral space parallel to the coronal axis (Fig. 1B). The OLIF interbody cages used had a width of 22 mm, an angulation of 12° and heights of 10, 12 and 14 mm (Clydesdale™ Spinal System; Medtronic, Memphis, TN, USA). They were meshed using 4-node tetrahedral elements of 0.5 mm and their material properties were set to polyether-ether-ketone (PEEK), with an elastic modulus (E) of 3.4 GPa and a Poisson's ratio (ν) of 0.4 (Faizan et al., 2014) (Fig. 1F). The cage models were positioned to match the middle of the superior endplate of L5, and a node-to-surface contact was established at the interface, ensuring a minimum distance of 0.5 mm and applying a Coulomb friction coefficient of 0.2. Subsequently, a distractive force was applied between L4 and L5 to expand the intervertebral body space while avoiding interference between the cage and endplate geometries. Finally, the loads were released following the activation of a node-to-surface contact between the cage and the vertebral endplates (Rastegar et al., 2020).

To assess spinal correction, several parameters were post-processed before and after simulated cage insertion, including slip, segmental lumbar lordosis (SLL), and the average disc height measured at five key locations on the endplates: the anterior-most, posterior-most, rightmost, leftmost, and center points. These reference points ensure a comprehensive assessment of disc height (Fig. 2A). Additionally, geometric indicators such as average foraminal height, foraminal area, and spinal canal diameter and area were computed to gauge potential indirect

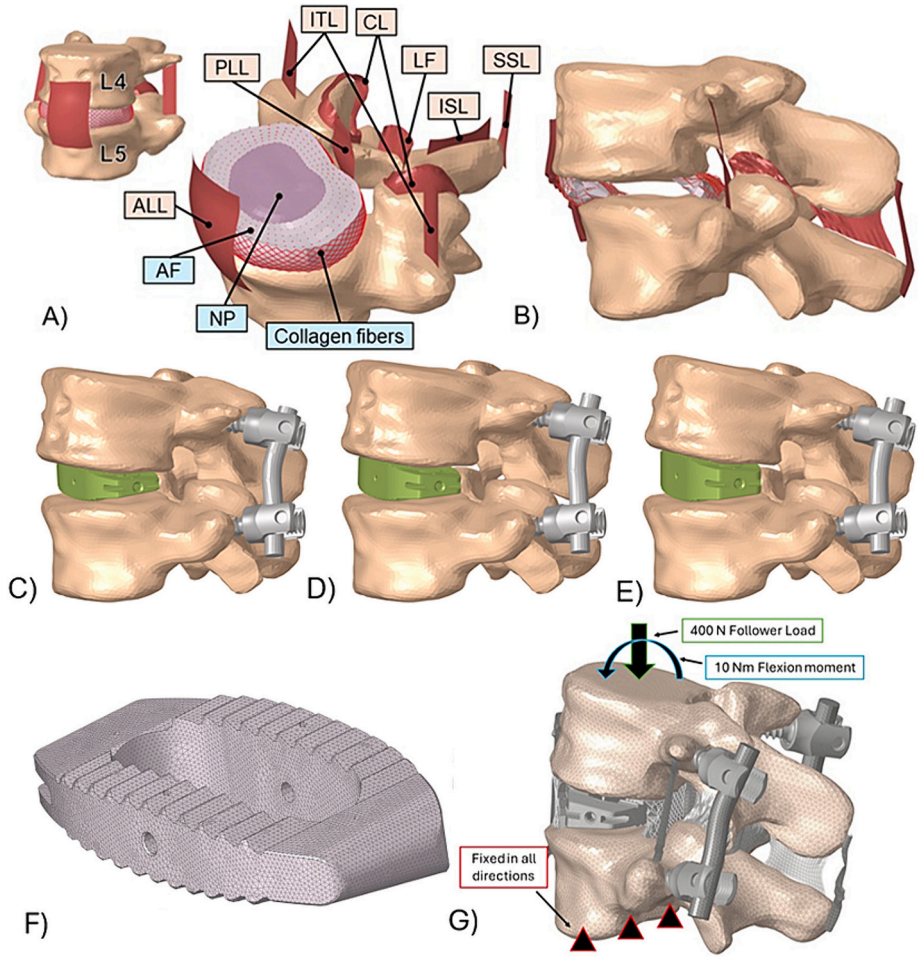

Fig. 1. Illustration of the A) asymptomatic L4-L5 finite element model, B) pathologic (grade I spondylolisthesis) model after discectomy and instrumented with C) 10-, D) 12-, and E) 14-mm cages combined with bilateral pedicle screw fixation and 6 mm rods (soft tissues omitted for clarity). F) Provides a detailed view of the interbody cage mesh. G) Displays the loading and boundary conditions applied to the models.

decompression. To measure the foraminal height, the distance between the most proximal point at the center of the L5 pedicle and the most distal point at the center of the L4 pedicle was recorded on each side (Fig. 3A). The spinal canal diameter was measured by visualizing a central sagittal cut of the canal and tracing the shortest distances between corresponding points on the L4 and L5 vertebrae on either side of the canal. The smallest of these two distances was used to evaluate the extent of spinal canal restriction caused by spondylolisthesis, as well as any changes resulting from the correction of vertebral slip (Fig. 3C). For the foraminal and spinal canal areas, enough points were selected along the contour to capture it with precision, and the areas were calculated using the Shoelace formula (Fig. 3B and D). For all measurements, the same points were used before and after surgery to ensure consistency. This approach minimizes the effect of viewing perspective on the results and maintains accuracy across the indicators.

To appreciate how extra millimeters in cage thickness can affect the outcomes, linear regressions were performed to examine the correlation between these postoperative decompression and realignment indicators and cage height. Following cage insertion, two pedicle screws (CD Horizon™ Solera™ 45 mm long, 6.5 mm diameter) were inserted in each vertebra according to the Magerl screw insertion technique (Song et al., 2021). Boolean operations were performed on the vertebra model to define its in-bone trajectory. The screws were meshed using 3-node shell elements sized at 0.25 mm and were modeled as rigid bodies interfacing with the bone, employing a Coulomb friction coefficient of 0.2 (Bianco et al., 2017). Rods with diameters of 4.75, 5.5 and 6 mm were meshed with 4-node tetrahedral elements (1 mm) before being inserted and tied to the screw head saddles (Fig. 1C). Material properties corresponding to titanium (E = 115 GPa, $\nu = 0.34$) were assigned to the screws and rods (Faizan et al., 2014).

This resulted in the collection of FEMs containing the models with a stand-alone (SA) cage or combined with BPS fixation and three possible rod sizes. The SA configuration was simulated to represent a virtual, non-clinical scenario with reduced stability, consistent with regulatory guidelines for Clydesdale's use alongside supplemental lumbar spine fixation systems. Subsequently, the 12 FEMs derived from one of the preoperative models were further used to assess the risk of cage subsidence in physiological loading conditions. A functional loading was simulated using a 400 N follower load and a 10 Nm flexion moment on the superior endplate of L4, while L5 was anchored in rotations and translations at the inferior endplate (Fig. 1G). Maximum Von Mises stresses and local compression of the vertebral endplates were measured to assess the risk of cage subsidence. Lastly, the simulations were repeated for an osteoporotic bone density. The significance of factors including cage height, the use of posterior fixation with BPS, and bone density was assessed using Repeated-Measures ANOVA tests. This statistical approach was chosen due to all scenarios being derived from a single geometric base model, making them interdependent. The assumptions of normality and sphericity were verified for each test.

All the simulations were performed using the explicit dynamic FEM solver RADIOSS 2020 (Altair Engineering Inc., Troy, USA) with kinetic relaxation to perform a quasi-static analysis (Bianco et al., 2017). The

Table 1
Material properties of bony elements, intervertebral disc and ligaments.

Bones								
Structures	Law	Density *(Kg/mm^3)*	Elastic modulus *(MPa)*	Poisson's ratio	Yield Stress *(MPa)*	Hardening modulus *(MPa)*	Failure plastic strain	Ref.
Cortical	Johnson-Cook	2E-6	2625	0.3	105	875	0.04	(Garo et al., 2011)
Trabecular		2E-7	48.75	0.25	1.95	16.3	0.04	

Intervertebral disc						
Structures	Law	Density *(Kg/mm^3*	Poisson's ratio	C_{10}	C_{01}	Ref.
Annulus Fibrosus	Mooney-Rivlin hyperelastic	1.2E-6	0.45	0.18	0.045	(Lee et al., 2000; Schmidt et al., 2007; Shirazi-Adl et al., 1986)
Nucleus		1E-6	0.495	0.12	0.03	
Collagen fibres	Force-displacement non-linear curves					

Ligaments									
Structures	Law	Density *(Kg/mm^3)*	Elastic modulus *(MPa)*	Poisson's ratio	Tangent modulus *(MPa)*	Tangent Poisson's ratio	Viscosity coefficient	Navier's constant	Ref.
ALL			11.4		10.0				
PLL			9.12		9.0				
ITL	Generalized		11.4		11.0				(El-Rich et al., 2009; Yang et al., 1998)
ISL	Maxwell-Kelvin-Voigt	1E-6	4.56	0.4	4.0	0.42	28	1E06	
LF			5.7		5.0				
SSL			8.55		8.0				
CL			22.8		22.0				

quasi-static state was confirmed by verifying that the system's kinetic energy remained significantly lower than the total energy (less than 1 %), with maximal strain rates ($\dot{\varepsilon}$) under 1 s^{-1} (Mattucci et al., 2012).

2.3. Model verification and validation

The previous methods and FEM were validated following the principles outlined in the ASME V&V40:2018 standard (ASME (2018)). The context of use (COU) was defined as the biomechanical analysis of indirect decompression in oblique lumbar intervertebral fusions applied to the treatment of grade I degenerative spondylolisthesis. The models were run under quasi-static loading conditions and enable different surgical scenarios to be compared on the basis of stresses on the vertebral endplates, as well as on geometric measurements of clinical interest (segmental lordosis, foraminal diameters, etc.). The aim of this study is to better understand how certain instrumental options and properties of the pathological spine can affect surgical outcome. It is a tool for comparing different scenarios, but is not, at this stage, being developed for use as a surgical planning tool. The level of risk associated with the models is evaluated as medium-low based on an analysis of influence on decision-making and consequences. The influence of the model is considered medium since this numerical biomechanical study provides insights and recommendations to support surgical decisions, but the final surgical decision primarily relies on the clinical experience of surgeons and the results of clinical studies. The consequences of the model are deemed low because the study's conclusions should not be directly applied in practice. The results contribute to advancing knowledge and complementing experimental studies and the experience of practitioners.

The SM2S, the main tool of this study, has been used in a multitude of contexts covered by more than twenty publications over the last fifteen years. In these past works, several elements of the model were the subject of verification and validation work, and many of whose results can be transferred to the present study context. In particular, the mechanical properties of the asymptomatic model under quasi-static loading conditions were validated by comparing the range of motion (ROM) with that of experimental cadaveric studies (Rastegar et al., 2020). Throughout this study, we have strengthened the validation of the model within its specific context. An experienced collaborating surgeon played a key role in validating the primary inputs and outputs. This involved meticulous examination of the discectomy, as well as the positioning of the cage and pedicle screws, to ensure they accurately mirrored the clinical OLIF approach. An assessment of the overall realism of the correction achieved in the simulated postoperative models was conducted. Additionally, the geometric models of instruments utilized to simulate the OLIF approach in this project are all derived from faithful representations of instruments commonly used in clinical practice. Finally, the main quantities of interest of this study, including stresses on vertebral endplates, disc height, slip, as well as foraminal height and area, were compared with those reported in other experimental and numerical studies interested in OLIF and indirect decompression. This comparison serves a dual purpose: first, to validate the reasonable realism and contextual adaptability of the preoperative pathological models developed; and second, to ensure that our findings align with clinically plausible outcomes.

3. Results

3.1. Evaluation of spinal realignment and potential indirect decompression

The simulated OLIF procedure was successfully performed on the five pathologic models. Fig. 2A, B, and C respectively display how the disc height, slip, and SLL changed before and after simulated cage insertion, and how it was affected by the cage height. Postoperative analysis following the simulated insertion of cages demonstrated significant improvements across all sizes. Initially, with the insertion of 10 mm cages, the average disc height increased to 12.0 ± 0.1 mm. Further

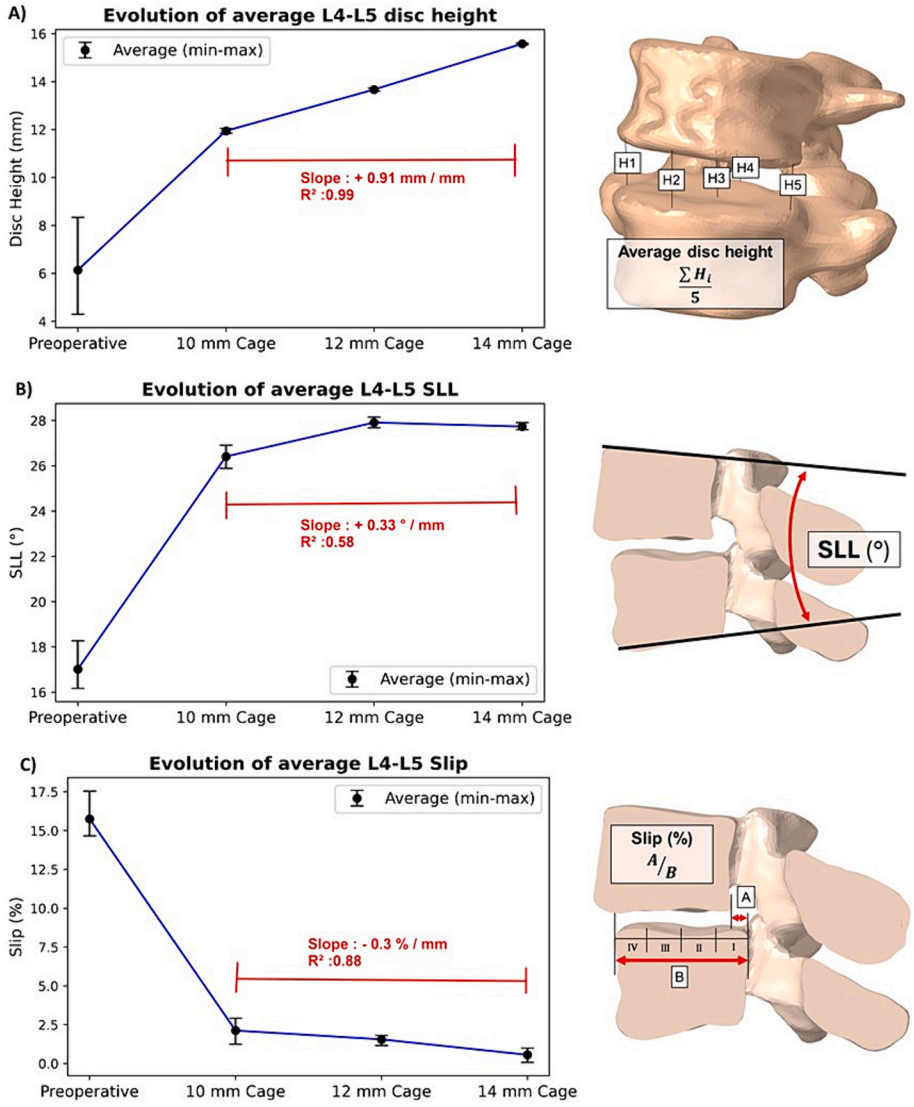

Fig. 2. Indicators of spinal realignment - Evolution of A) disc height, B) SLL, and C) slip from preoperative to OLIF instrumentation with 10-, 12- and 14-mm cages in the 5 pathologic models.

enhancements were observed with larger cage sizes, with the average disc height increasing to 13.7 ± 0.1 mm for 12 mm cages and 15.6 ± 0.1 mm for 14 mm cages. Across all cage heights, the average postoperative SLL was 27.3° (10 mm, 26.4°, 12 mm, 27.9°, 14 mm, 27.7°), with a slip of 1.4 % (10 mm, 2.1 %, 12 mm, 1.6 %, 14 mm, 0.6 %).

Fig. 3A and C illustrate the evolution of foraminal height and spinal canal diameter throughout the OLIF simulation. Preoperatively, foraminal diameter averaged 13.1 ± 1.3 mm and spinal canal diameter averaged 16.2 ± 0.4 mm. Foraminal area measured 96 ± 12 mm^2 and spinal canal area measured 764 ± 20 mm^2, as depicted in Fig. 3B and D respectively. Post-cage insertion, significant expansions were observed across all cage sizes, with foraminal diameter increasing to 14.8 ± 0.2 mm (10 mm), 16.0 ± 0.1 mm (12 mm), and 18.0 ± 0.1 mm (14 mm). This was accompanied by notable increases in foraminal area, with measurements reaching 104 ± 3 mm^2, 114 ± 1 mm^2, and 131 ± 1 mm^2 respectively. Likewise, spinal canal diameter expanded to 19.9 ± 0.1 mm (10 mm), 20.2 ± 0.1 mm (12 mm), and 21.2 ± 0.1 mm (14 mm), accompanied by increases in spinal canal area to 789 ± 5 mm^2, 807 ± 2 mm^2, and 844 ± 2 mm^2 respectively.

Linear regressions were computed to assess the relationship between spinal realignment and indirect decompression indicators with cage height. Figs. 2 and 3 display the determination coefficient and the linear slopes. The slope represents the extent of variation in these parameters per additional mm of cage height within the tested range of cage heights (10, 12, and 14 mm).

3.2. Assessment of cage subsidence risk

Table 2 provides an overview of the maximum Von-Mises stresses and displacements on the cortical endplate of L5 under a combined compression-flexion loading, accounting for both normal and osteoporotic bone densities. An illustration of the distribution of these stresses and displacements is available in the supplementary materials to this article.

To determine the significance of various factors such as cage height, with or without posterior fixation with BPS, and bone density, Repeated-Measures ANOVA tests were conducted. Results revealed a significant impact of posterior fixation ($P < 0.001$) on both stresses and displacements. The addition of BPS fixation with increased rod diameter substantially reduced both stresses and displacements, with reductions of up to 46 % and 69 %, respectively, compared to SA cage configurations.

Furthermore, an increase in cage height corresponded to a general rise in stresses ($P = 0.029$) and displacements ($P = 0.18$). Lower bone density had a limited effect on endplate stresses ($P = 0.18$), resulting in a

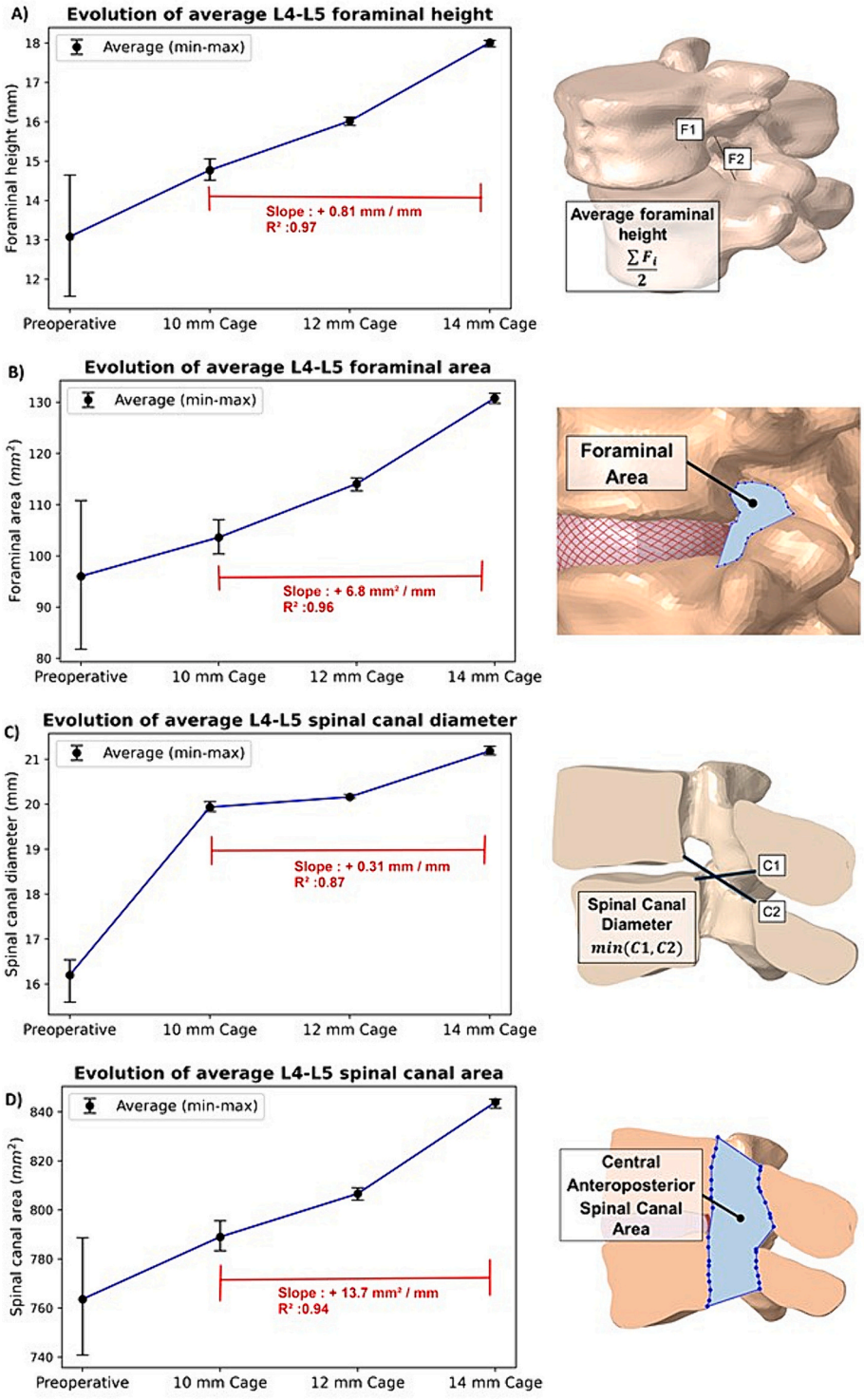

Fig. 3. Indicators of indirect decompression - Evolution of A) foraminal diameter, B) foraminal area, C) spinal canal diameter, and D) spinal canal area from preoperative to OLIF instrumentation with 10-, 12- and 14-mm cages in the 5 pathologic models.

3 % average reduction compared to normal bone density conditions. However, it significantly amplified displacements ($p < 0.001$), resulting in an increase ranging from 43 % to 85 % (averaging 63 %) compared to normal bone density scenarios.

3.3. Comparative analysis of quantities of interest

The results of two clinical studies (Mahatthanatrakul et al., 2022; Sato et al., 2017), which concentrate on OLIF and indirect decompression for treating spinal stenosis and degenerative spondylolisthesis, were gathered to compare them with the average values seen in this study. The foraminal height, vertebral slip, disc height, and foraminal area measured on the FEMs were compared with the preoperative and postoperative values reported in these clinical studies, totaling more than 60 cases. Fig. 4 illustrates that the values measured in this numerical study are comparable in range with the reality observed clinically. Additionally, several recent numerical studies that focused on the OLIF approach were chosen to validate the magnitude of stresses

Table 2
Maximum Von-Mises stress and maximum compression displacements on L4-L5 Endplates (under 10 Nm flexion and a 400 N gravitational load) for normal bone density and osteoporosis in stand-alone (SA) and bilateral pedicle screw (BPS) fixation setups with cages of 10,12 and 15 mm heights and rods of 4.75, 5.5, and 6 mm diameters.

	Maximum Von-Mises Stress on L4-L5 Endplates (MPa)							
	Normal bone density				Osteoporosis			
	SA	BPS (4.75 mm Rods)	BPS (5.5 mm Rods)	BPS (6 mm Rods)	SA	BPS (4.75 mm Rods)	BPS (5.5 mm Rods)	BPS (6 mm Rods)
10 mm cage (12°)	62.6	39.6	36.3	33.6	51.9	44.9	39.5	35.2
12 mm cage (12°)	61.8	46.2	43.7	41.2	53.1	48.2	43.9	40.2
14 mm cage (12°)	65.5	47.9	46.1	45.0	54.2	45.6	43.7	42.2

	Maximum displacement on L4-L5 Endplates (mm)							
	Normal bone density				Osteoporosis			
	SA	BPS (4.75 mm Rods)	BPS (5.5 mm Rods)	BPS (6 mm Rods)	SA	BPS (4.75 mm Rods)	BPS (5.5 mm Rods)	BPS (6 mm Rods)
10 mm cage (12°)	0.64	0.23	0.22	0.20	0.98	0.43	0.38	0.34
12 mm cage (12°)	0.58	0.26	0.25	0.23	0.90	0.46	0.41	0.37
14 mm cage (12°)	0.61	0.31	0.29	0.28	0.89	0.51	0.46	0.43

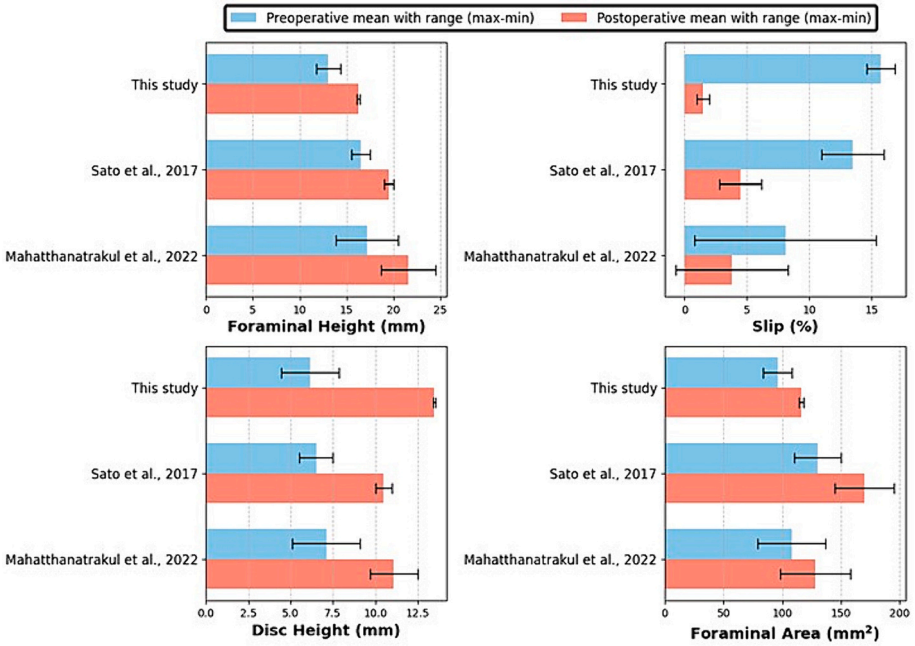

Fig. 4. Comparison of the range of measured foraminal height, slip, disc height and foraminal height with the values reported in experimental studies interested in OLIF and indirect decompression.

measured on the vertebral endplates. Our results fall within a similar range to the values reported in other similar studies (Cai et al., 2022; Fan et al., 2023; Fang et al., 2020; Xue and Wu, 2023; Zhang et al., 2022).

4. Discussion

The evaluation of spinal realignment and potential indirect decompression following the simulated OLIF procedure yielded valuable quantified insights into the efficacy and outcomes of this surgical intervention. Our findings indicate successful execution of the procedure on the five pathologic models, as evidenced by the notable improvements observed postoperatively across all instrumentation scenarios and preoperative disc heights. In terms of slip and SLL, similar outcomes were obtained across all tested cage heights (10 mm, 12 mm, and 14 mm), with slightly better results observed with increased cage height. Variations in required distraction forces may account for slight differences in final vertebral sagittal positioning and subsequent postoperative slip, despite similar cage placement. Across all cages, an average postoperative slip under 2 % indicates that the simulated approach successfully managed to achieve a good sagittal realignment. Similarly, SLL is likely influenced by the angulation of the cage and the specific geometry and contact points of the vertebral endplates with the cage. Since all cages employed a 12° angulation, it's reasonable to expect similar resultant lordosis. Although the primary distinction among the cages was their heights, there were also slight variations in their geometry, particularly regarding the contact points with the vertebrae. These differences may contribute to the observed variability in outcomes.

As anticipated from a geometric perspective, there was a strong and positive linear correlation between postoperative disc height and cage height ($R^2 = 0.99$). Within the range of cage heights utilized, we observed that each additional millimetre of cage height led to an average

increase of 0.91 mm in postoperative disc height. Although it may initially seem counterintuitive that postoperative disc height does not precisely correspond to cage height (at least prior to any subsidence), this can be elucidated by considering that the average disc height is influenced not only by the specified height of the cage but also by its specific geometry, including angulation, anterior and posterior height, and its interaction with the patient-specific endplate geometry. Regarding the dimensions of the foramens and spinal canal, our findings also align with the expectation that taller cages would lead to larger enlargements. We observed strong positive linear relationships between cage height and the area and diameters of these openings, with determination coefficients (R^2) ranging from 0.87 to 0.97. As illustrated in Fig. 4, the measured values for the geometric indicators of realignment and decompression on the FEMs generally align reasonably well with clinically plausible observations.

In assessing the potential for cage subsidence, our study investigated the maximum Von-Mises stresses and displacements on the vertebral endplates across different bone densities, all subjected to the same physiological loading conditions. The results underscore the significance of factors such as posterior fixation, cage height, and bone density in influencing stress distribution and subsidence risk. While all measured stresses were significantly below the cortical compressive yield stress range (131–224 MPa in compression) (Kundu et al., 2014), there was a significant reduction in stresses and displacements with the implementation of BPS fixation, particularly as the rod diameter increased. This highlights the importance of supplementary stabilization instrumentation in enhancing stability and minimizing subsidence risk, aligning with findings from numerous prior experimental and numerical studies (Ouyang et al., 2023; Yang et al., 2022). This could hold significant implications, particularly in cases of osteoporotic bone densities, for which we observed stress levels similar to those in normal bone density, but significantly greater displacements on the endplates (up to 85 % more). Besides, higher cage height correlated with an overall increase in stresses. This can be attributed to the augmented intervertebral distraction required for the insertion and positioning of taller cages, consequently leading to heightened compression forces at the interface between the bone and cage, induced by the tightening of soft tissues. Such findings can bear significant clinical relevance as the risk of subsidence implies a potential compromise in the correction and decompression achieved immediately post-surgery. Upon comparing the maximum stresses on cortical endplates measured in our study for the SA and BPS constructs with those documented in 11 additional OLIF FEM studies, our findings fell squarely within the average range. It is important to caution that significant variability exists among other studies, stemming from differences in modelling hypotheses, geometric representations, loading conditions and measurement methods.

The study's approach involved simplifications and approximations in the modelling and simulations. For instance, the cortical and trabecular bones were modeled as homogeneous isotropic materials, and the geometry and mechanical properties were based on a generic model. This study did not account for nervous structures, osteophytes, hyaline cartilage layers on the vertebral endplates and facets, and other anatomical complexities, which could modify and impact the applicability of the findings. Incorporating these features will be considered for future work to improve model accuracy. This study employed a simplified simulation process by fixing L5 and translating L4 to mimic preoperative pathological conditions with varying intervertebral disc heights, as a first step towards creating more representative pathological models. While this approach is a foundational method, future studies will aim to refine these models further by integrating clinical data to enhance the accuracy and realism of the biomechanical simulations. Additionally, the simulations only depict the patient's state immediately after surgery under quasi-static loading, which may differ from postoperative functional loads of daily activities. Hence, these results offer a general perspective and should be compared with experimental data. Nonetheless, these findings provide a rigorously systematic quantitative overview of the factors influencing correction, decompression, and subsidence risk in OLIF procedures, facilitating more informed surgical planning and optimization of outcomes.

5. Conclusion

This study provides quantitative insights into the biomechanics of OLIF procedures, offering valuable guidance for surgical planning and optimization of outcomes. We found that using taller cages can improve spinal realignment and decompression, but also increase the risk of cage subsidence. Posterior fixation with BPS and larger rod diameters significantly reduces subsidence risk, particularly in osteoporotic cases. The tools developed in this study demonstrated a great potential for evaluating the biomechanics of OLIF. Future planned research includes utilizing these methods to simulate clinical cases, with the goal of validating the findings and bolstering the model's credibility. The model could be adapted to include nervous structures and delve further into representing pathological conditions, thus providing more accurate simulations of real-world surgical scenarios. Moreover, exploring the impact of alternative implants and stabilization methods in OLIF procedures could provide valuable knowledge.

CRediT authorship contribution statement

Mathieu Chayer: Writing – original draft, Validation, Methodology, Investigation, Formal analysis, Conceptualization. **Philippe Phan:** Writing – review & editing, Validation, Supervision, Methodology, Conceptualization. **Pierre-Jean Arnoux:** Writing – review & editing, Supervision, Methodology, Conceptualization. **Zhi Wang:** Writing – review & editing. **Carl-Éric Aubin:** Writing – review & editing, Supervision, Project administration, Methodology, Funding acquisition, Conceptualization.

Declaration of competing interest

The authors declare the following financial interests/personal relationships which may be considered as potential competing interests.

Carl-Eric Aubin reports academic R&D support from the Natural Sciences and Engineering Research Council of Canada (NSERC) (industrial research chair program with Medtronic of Canada). Mathieu Chayer reports financial support was provided by Quebec Research Fund Nature and Technology. Mathieu Chayer reports financial support was provided by TransMedTech Institute. Mathieu Chayer reports financial support was provided by Natural Sciences and Engineering Research Council of Canada. If there are other authors, they declare that they have no known competing financial interests or personal relationships that could have appeared to influence the work reported in this paper.

Appendix A. Supplementary data

Supplementary data to this article can be found online at https://doi.org/10.1016/j.clinbiomech.2024.106352.

References

ASME, 2018. V&V40-2018: Assessing Credibility of Computational Modeling Through Verification and Validation: Application to Medical Devices.

Bereczki, F., Turbucz, M., Kiss, R., Eltes, P.E., Lazary, A., 2021. Stability Evaluation of Different Oblique Lumbar Interbody Fusion Constructs in Normal and Osteoporotic Condition - A Finite Element Based Study. Front. Bioeng. Biotechnol. 9, 749914. https://doi.org/10.3389/fbioe.2021.749914.

Bianco, R.J., Arnoux, P.J., Wagnac, E., Mac-Thiong, J.M., Aubin, C., 2017. Minimizing Pedicle Screw Pullout Risks: A Detailed Biomechanical Analysis of Screw Design and Placement. Clin. Spine Surg. 30 (3), E226–e232. https://doi.org/10.1097/bsd.0000000000000151.

Cai, X.Y., Bian, H.M., Chen, C., Ma, X.L., Yang, Q., 2022. Biomechanical study of oblique lumbar interbody fusion (OLIF) augmented with different types of instrumentation: a finite element analysis. J. Orthop. Surg. Res. 17 (1), 269. https://doi.org/10.1186/s13018-022-03143-z.

El-Rich, M., Arnoux, P.J., Wagnac, E., Brunet, C., Aubin, C.E., 2009. Finite element investigation of the loading rate effect on the spinal load-sharing changes under impact conditions. J. Biomech. 42 (9), 1252–1262. https://doi.org/10.1016/j.jbiomech.2009.03.036.

Faizan, A., Kiapour, A., Kiapour, A.M., Goel, V.K., 2014. Biomechanical analysis of various footprints of transforaminal lumbar interbody fusion devices. J. Spinal Disord. Tech. 27 (4), E118–E127. https://doi.org/10.1097/BSD.0b013e3182a11478.

Fan, K., Zhang, D., Xue, R., Chen, W., Hou, Z., Zhang, Y., Meng, X., 2023. Biomechanical analysis of double-level oblique lumbar fusion with different types of fixation: a finite element-based study. Orthop. Surg. 15 (5), 1357–1365. https://doi.org/10.1111/os.13703.

Fang, G., Lin, Y., Wu, J., Cui, W., Zhang, S., Guo, L., Huang, W., 2020. Biomechanical Comparison of Stand-Alone and Bilateral Pedicle Screw Fixation for Oblique Lumbar Interbody Fusion Surgery—A Finite Element Analysis. World Neurosurg. 141, e204–e212. https://doi.org/10.1016/j.wneu.2020.05.245.

Ferreira, M.L., Luca, K.D., Haile, L.M., Steinmetz, J.D., Culbreth, G.T., Cross, M., 2023. Global, regional, and national burden of low back pain, 1990-2020, its attributable risk factors, and projections to 2050: a systematic analysis of the Global Burden of Disease Study 2021. Lancet Rheumatol. 5 (6), e316–e329. https://doi.org/10.1016/s2665-9913(23)00098-x.

Garo, A., Arnoux, P.J., Wagnac, E., Aubin, C.E., 2011. Calibration of the mechanical properties in a finite element model of a lumbar vertebra under dynamic compression up to failure. Med. Biol. Eng. Comput. 49 (12), 1371–1379. https://doi.org/10.1007/s11517-011-0826-z.

Guo, H.-Z., Tang, Y.-C., Guo, D.-Q., Luo, P.-J., Li, Y.-X., Mo, G.-Y., Zhang, S.-C., 2020. Stability Evaluation of Oblique Lumbar Interbody Fusion Constructs with Various Fixation Options: A Finite Element Analysis Based on Three-Dimensional Scanning Models. World Neurosurg. 138, e530–e538. https://doi.org/10.1016/j.wneu.2020.02.180.

Hao, J., Tang, X., Jiang, N., Wang, H., Jiang, J., 2023. Biomechanical stability of oblique lateral interbody fusion combined with four types of internal fixations: finite element analysis. Front. Bioeng. Biotechnol. 11, 1260693. https://doi.org/10.3389/fbioe.2023.1260693.

Iwasaki, M., Hayase, H., Takamiya, S., Yamazaki, K., 2022. Preoperative dorsal disc height is a predictor of indirect decompression effect through oblique lateral interbody fusion in lumbar degenerative stenosis. Medicine (Baltimore) 101 (41), e31020. https://doi.org/10.1097/md.0000000000031020.

Kundu, J., Pati, F., Shim, J.H., Cho, D.W., 2014. 12 - Rapid prototyping technology for bone regeneration. In: Narayan, Dans R. (Ed.), Rapid Prototyping of Biomaterials, (Second Edition). Woodhead Publishing, pp. 289–314.

Lee, C.K., Kim, Y.E., Lee, C.S., Hong, Y.M., Jung, J.M., Goel, V.K., 2000. Impact response of the intervertebral disc in a finite-element model. Spine (Phila Pa 1976) 25 (19), 2431–2439. https://doi.org/10.1097/00007632-200010010-00003.

Liu, Z.-X., Gao, Z.-W., Chen, C., Liu, Z.-Y., Cai, X.-Y., Ren, Y.-N., Yang, Q., 2022. Effects of osteoporosis on the biomechanics of various supplemental fixations co-applied with oblique lumbar interbody fusion (OLIF): a finite element analysis. BMC Musculoskelet. Disord. 23 (1), 794. https://doi.org/10.1186/s12891-022-05645-7.

Lu, T., Lu, Y., 2019. Comparison of Biomechanical Performance Among Posterolateral Fusion and Transforaminal, Extreme, and Oblique Lumbar Interbody Fusion: A Finite Element Analysis. World Neurosurg. 129, e890–e899. https://doi.org/10.1016/j.wneu.2019.06.074.

Mahatthanatrakul, A., Kotheeranurak, V., Lin, G.X., Hur, J.W., Chung, H.J., Lokanath, Y. K., Kim, J.S., 2022. Do Obliquity and Position of the Oblique Lumbar Interbody Fusion Cage Influence the Degree of Indirect Decompression of Foraminal Stenosis? J. Korean Neurosurg. Soc. 65 (1), 74–83. https://doi.org/10.3340/jkns.2021.0105.

Mattucci, S.F., Moulton, J.A., Chandrashekar, N., Cronin, D.S., 2012. Strain rate dependent properties of younger human cervical spine ligaments. J. Mech. Behav. Biomed. Mater. 10, 216–226. https://doi.org/10.1016/j.jmbbm.2012.02.004.

Ouyang, P., Tan, Q., He, X., Zhao, B., 2023. Computational comparison of anterior lumbar interbody fusion and oblique lumbar interbody fusion with various supplementary fixation systems: a finite element analysis. J. Orthop. Surg. Res. 18 (1), 4. https://doi.org/10.1186/s13018-022-03480-z.

Polikeit, A., Nolte, L.P., Ferguson, S.J., 2003. The effect of cement augmentation on the load transfer in an osteoporotic functional spinal unit: finite-element analysis. Spine (Phila Pa 1976) 28 (10), 991–996. https://doi.org/10.1097/01.Brs.0000061987.71624.17.

Qin, Y., Zhao, B., Yuan, J., Xu, C., Su, J., Hao, J., Wang, Y., 2022. Does Cage Position Affect the Risk of Cage Subsidence After Oblique Lumbar Interbody Fusion in the Osteoporotic Lumbar Spine: A Finite Element Analysis. World Neurosurg. 161, e220–e228. https://doi.org/10.1016/j.wneu.2022.01.107.

Rastegar, S., Arnoux, P.J., Wang, X., Aubin, C., 2020. Biomechanical analysis of segmental lumbar lordosis and risk of cage subsidence with different cage heights and alternative placements in transforaminal lumbar interbody fusion. Comput. Meth. Biomech. Biomed. Engin. 23 (9), 456–466. https://doi.org/10.1080/10255842.2020.1737027.

Sato, J., Ohtori, S., Orita, S., Yamauchi, K., Eguchi, Y., Ochiai, N., Takahashi, K., 2017. Radiographic evaluation of indirect decompression of mini-open anterior retroperitoneal lumbar interbody fusion: oblique lateral interbody fusion for degenerated lumbar spondylolisthesis. Eur. Spine J. 26 (3), 671–678. https://doi.org/10.1007/s00586-015-4170-0.

Schmidt, H., Kettler, A., Heuer, F., Simon, U., Claes, L., Wilke, H.J., 2007. Intradiscal pressure, shear strain, and fiber strain in the intervertebral disc under combined loading. Spine (Phila Pa 1976) 32 (7), 748–755. https://doi.org/10.1097/01.brs.0000259059.90430.c2.

Shirazi-Adl, A., Ahmed, A.M., Shrivastava, S.C., 1986. A finite element study of a lumbar motion segment subjected to pure sagittal plane moments. J. Biomech. 19 (4), 331–350. https://doi.org/10.1016/0021-9290(86)90009-6.

Song, M., Sun, K., Li, Z., Zong, J., Tian, X., Ma, K., Wang, S., 2021. Stress distribution of different lumbar posterior pedicle screw insertion techniques: a combination study of finite element analysis and biomechanical test. Sci. Rep. 11 (1), 12968. https://doi.org/10.1038/s41598-021-90686-6.

Wagnac, E., Arnoux, P.-J., Garo, A., Aubin, C.-E., 2012. Finite element analysis of the influence of loading rate on a model of the full lumbar spine under dynamic loading conditions. Med. Biol. Eng. Comput. 50 (9), 903–915. https://doi.org/10.1007/s11517-012-0908-6.

Xu, W., Liu, W., Zhong, F., Peng, Y., Liu, X., Yu, L., 2023. Efficacy of OLIF combined with pedicle screw internal fixation for lumbar spinal stenosis on spinal canal changes before and after surgery. J. Orthop. Surg. Res. 18 (1), 724. https://doi.org/10.1186/s13018-023-04209-2.

Xue, S., Wu, T., 2023. Biomechanical Performances of an Oblique Lateral Interbody Fusion Cage in Models with Different Bone Densities: A Finite Element Analysis. Indian J. Orthop. 57 (1), 86–95. https://doi.org/10.1007/s43465-022-00775-5.

Yang, K.H., Z. F, Luan, F., Zhao, L., Begeman, P.C., 1998. Development of a Finite Element Model of the Human Neck. SAE Technical Paper Series.

Yang, Z.Q., Cai, P., Li, J.C., Wang, X.D., Xie, T.H., Pu, X.X., Song, Y.M., 2022. Stepwise reduction of bone mineral density increases the risk of cage subsidence in oblique lumbar interbody fusion patients biomechanically: an in-silico study. BMC Musculoskelet. Disord. 23 (1), 1083. https://doi.org/10.1186/s12891-022-06049-3.

Zhang, S., Liu, Z., Lu, C., Zhao, L., Feng, C., Wang, Y., Zhang, Y., 2022. Oblique lateral interbody fusion combined with different internal fixations for the treatment of degenerative lumbar spine disease: a finite element analysis. BMC Musculoskelet. Disord. 23 (1), 206. https://doi.org/10.1186/s12891-022-05150-x.

Zhang, S., Zhang, Y., Huang, L., Zhang, S., Lu, C., Liu, Z., Wang, Z., 2023. Oblique lateral interbody fusion with internal fixations in the treatment for cross-segment degenerative lumbar spine disease (L2-3 and L4-5) finite element analysis. Sci. Rep. 13 (1), 17116. https://doi.org/10.1038/s41598-023-43399-x.

Zhong, Y., Wang, Y., Zhou, H., Wang, Y., Gan, Z., Qu, Y., Jiang, W., 2023. Biomechanical study of two-level oblique lumbar interbody fusion with different types of lateral instrumentation: a finite element analysis. Front. Med. (Lausanne) 10. https://doi.org/10.3389/fmed.2023.1183683.